A Taylor basis for kinematic nonlinear real-time simulations. Part I: The complete modal derivatives

Andersen, Sebastian; Poulsen, Peter Noe

Published in:
Earthquake Engineering and Structural Dynamics

Link to article, DOI:
10.1002/eqe.3176

Publication date:
2019

Document Version
Peer reviewed version

2019; **00**:1–20

A Taylor Basis for Kinematic Nonlinear Real-time Simulations. Part I: The Complete Modal Derivatives

S. Andersen*† and P. N. Poulsen ‡

Department of Civil Engineering, Technical University of Denmark, 2800 Kgs. Lyngby, Denmark

SUMMARY

Despite todays computational power, only small nonlinear numerical substructures may be simulated in real time. The size restriction on the substructures in nonlinear finite element analysis is primarily due to the time-consuming evaluation of the internal restoring forces which is performed element-by-element in every iteration step. The present work constitutes the first of two papers presenting a method to simulate kinematic nonlinear structures more efficiently. It involves applying a reduced basis with modal derivatives representing the nonlinearities of the system in an efficient way. Previously, the modal derivatives have been determined from a set of approximate governing equations. In the present paper a novel set of equations governing the complete modal derivatives is derived. This is done by introducing a Taylor series into the free undamped kinematic nonlinear equations of motion. Also the approximate governing equations are improved by introducing a novel geometric restriction. By way of an example it is shown that only the modal derivatives determined from the complete set of equations are consistent with the Taylor series. In the second paper it is shown that the novel modal derivatives may be used in a so-called Taylor basis and that they improve the computational time and stability significantly.

Received . . .

KEY WORDS: Basis Projection; Modal Derivatives; Finite Element Analysis; Kinematic Nonlinearities; Real-time Simulations

1. INTRODUCTION

The rapid increase in computational speed over the last decades has lead to increased application of real-time simulations in the industry and research community within engineering fields. For real-time simulations the time spent producing the model output is shorter than or equal to the simulated time. Real-time simulations are applied in engineering fields, such as aircraft simulation, motor drive controller design, space robot integration, computer graphics and structural testing, see [1–3].

The motivation for the present work relates specifically to the engineering field of hybrid testing in which physical and numerical substructures are combined, see e.g. [4–9]. The principle of the method is to partition a test structure into two parts that run in parallel and which are coupled through a continuously interchange of data. One is a physical part of the structure which is considered to be a black box displaying complicated structural behavior. This substructure must be tested in a physical test setup. The response of the other part is well understood and does not have to be tested physically. Instead it can be modeled numerically by e.g. the Finite Element Method (FEM). If the behavior of the physical substructure is rate dependent, then the structural test and the corresponding

*Correspondence to: Sebastian Andersen, Department of Civil Engineering, Technical University of Denmark, 2800 Kgs. Lyngby, Denmark. Tel.: +45 25 50 48, E-mail: seba@byg.dtu.dk
†Postdoc
‡Associate Professor

numerical simulations have to be performed in real-time, and the test is then often referred to as a real-time hybrid simulation (RTHS).

The present work focus purely on numerical real-time simulations of kinematic nonlinear structures, with the overall aim to formulate a general method for improving the simulation efficiency. Thus, the coupling of physical and numerical substructures which appears in e.g. RTHS is not considered.

One crucial aspect for real-time simulations of dynamic systems to be successful is that the time integration is robust, accurate and fast. However, when nonlinear behavior is included, the real-time execution requirement significantly limits the size of the numerical model. An example of this size limitation is seen in RTHS where the largest number of DOFs included in nonlinear tests today is 514, see [10]. For many applications this is considered a modest model size. In general the size restriction in real-time FEM simulations is mainly due to a time consuming evaluation of the nonlinear internal restoring forces element-by-element, followed by assembling of the global set of equations before conducting each time step. By increasing the size of the numerical model, the assembly time is obviously increased as well. Simultaneously, when increasing the size and complexity of the model higher frequencies are introduced. This calls for smaller time steps in the integration schemes in order to maintain stability and accuracy, which increase the frequency of assembling the matrices and thereby also the computational time.

An efficient way to reduce the computational time of nonlinear systems is to reduce the number of DOFs in the model. This is also referred to as a reduced order model. The reduction in DOFs can be achieved by projecting the discretized nonlinear equations of motion (EOMs) onto a subspace represented by a so-called reduced basis, see e.g. [11]. The concept is well known from linear theory, and provides a simple way to reduce the number of DOFs and at the same time cuts off some of the non-physical higher frequency content in the model. The first use of the concept for kinematic nonlinear structural systems can be dated back to the work in [12, 13] where so-called mode shape vectors constituted the basis vectors. Basis projection is also used in real-time applications, e.g. in the field of computer graphics simulations, for medical purposes and also for linear and nonlinear RTHS, see [2, 14–16]. The concept of basis projection also constitutes the core of the present work.

In [17] an overview and evaluation of the most commonly used basis vectors applied for kinematic nonlinear structures, considering robustness and accuracy, is presented. Among these are linear normal modes (also known as the system mode shapes), modal derivatives (MDs) [18], Ritz vectors [19], and vectors based on the proper orthogonal decomposition (POD) method [20–22]. The work in [17] concludes that the POD vectors perform the best, with the system mode shapes as a good alternative. However, the POD vectors are generated from a number of data snapshots taken from a full model simulation prior to the actual simulation. This limits its field of application to areas where test simulations are possible. However, this is not possible in a field such as RTHS where the FEM model is required before the test can run. Thus, for the basis projection to be generally usefull the system mode shapes and their MDs appear as a natural basis choice, as these can be generated from the full FEM model prior to the simulations.

The MDs were introduced in [18, 23] where a set of equations governing the first order MDs were derived by differentiating the linearized eigenvalue problem. However, when a linearized system of equations is differentiated, the result will only represent an approximation of the actual derivative. This leads to a set of approximate governing equations including a singular matrix from which the MDs cannot be determined directly. The most common approach to circumvent this problem has been to neglect the inertia of the system, leading to so-called static modal derivatives, see e.g. [2, 18, 24–26]. Alternatively, the authors of [27] suggest a numerical approach where the MDs are evaluated as the difference between two tangent modes at two equilibrium stages separated by a small displacement increment. Furthermore, [18, 27] discuss the possibility of counteracting the singularity by constraining a component of the MDs, and determining the remaining components through a reduced set of equations. In [28] a perturbation method is used to derive a set of equations from which the MDs can be determined. However, common for all of the above mentioned approaches, is that they lead to approximate solutions with singularity issues.

The present work constitutes the first of two papers with focus on developing a reduced basis method for efficient simulations of dynamically loaded kinematic nonlinear systems. To make the method as generally applicable as possible a basis including system mode shapes and MDs is considered. The basis is organized from a Taylor series that predicts a fixed relation between the modal co-ordinates of the system mode shapes and the MDs. Thus, the number of unknowns in the formulation is equal to the number of included mode shapes only. This minimizes the computational cost significantly, since the full solution is known solely by determining the modal co-ordinates of the system mode shapes.

The focus of the present paper is dedicated to deriving a set of improved non-singular systems of equations governing the first order MDs to be used in the Taylor basis formulation. This is obtained by applying perturbation methods where a Taylor series is introduced into the free undamped kinematic nonlinear EOMs, which leads to equations of different orders to be solved. In the given context the second order equations are of special interest, as they represent the systems of equations governing the first order MDs. The novel equations are referred to as the complete governing system of equations and the MDs as the complete MDs. The complete MDs are compared with an improved version of the MDs governed by the singular equations introduced in [18, 23]. The improvement consist of an additional condition introduced by use of the Lagrange multiplier method, that removes the singularity of the equations.

In the second paper the Taylor series is organized and used as a projection basis including the complete MDs derived in the present paper. It is illustrated that the basis formulation can improve both the computational efficiency and the numerical stability significantly.

In the following section, the general formulation of the governing EOMs is presented together with an illustrative example of the effects of kinematic nonlinearities. In Section 3 the principle of basis projection together with the derivation of the two novel systems of equations governing the MDs are considered. Then, in Section 4 an example considering a kinematically highly nonlinear cable exposed to harmonic loading is given. The example is used to demonstrate that only the complete MDs are consistent with the prediction of the Taylor series. Finally, in Section 5 a conclusion is given.

2. THE GOVERNING KINEMATIC NONLINEAR EQUATIONS OF MOTION

In the following section, the general governing EOMs in discretized form are presented. The general formulation is supplemented with a specific example considering the Euler-Bernoulli beam element with a nonlinear strain measure. Moreover, the Euler-Bernoulli beam is used to illustrate the effect of kinematic nonlinearities on a cantilever beam.

2.1. The Governing Equations of Motion

The starting point of a numerical structural dynamic analysis is to consider the discretized EOMs in physical co-ordinates containing n DOFs, see (1). These are found by use of *Calculus of Variation* applied as *the principle of virtual work*.

$$\mathbf{M}\ddot{\mathbf{V}} + \mathbf{C}\dot{\mathbf{V}} + \mathbf{g}(\mathbf{V}) = \mathbf{F}(t) \tag{1}$$

The elements in the EOMs in (1) consist of the vector $\mathbf{V}$ which is of dimensions $n\times 1$ and represents the nodal displacements in global format, $\mathbf{M}$ and $\mathbf{C}$ which are $n \times n$ mass and damping matrices, $\mathbf{F}(t)$ which is an $n\times 1$ external load vector expressed as a function of time t and $\mathbf{g}(\mathbf{V})$ which is an $n\times 1$ nonlinear vector in $\mathbf{V}$ containing the internal nodal restoring forces. Furthermore, the notation $\dot{()} = d()/dt$ defines a time derivative. The internal nodal restoring forces are also expressed as the secant stiffness matrix, $\mathbf{K}_s(\mathbf{V})$, multiplied by the displacement vector

$$\mathbf{g}(\mathbf{V}) = \mathbf{K}_s(\mathbf{V})\mathbf{V} \tag{2}$$

Furthermore, to describe the present stiffness of the system at a given displacement state $\mathbf{V}_0$ the tangent stiffness matrix $\mathbf{K}_T$ is used. This is defined as

$$\mathbf{K}_T(\mathbf{V}_0) = \left.\frac{\partial \mathbf{g}(\mathbf{V})}{\partial \mathbf{V}}\right|_{\mathbf{V}_0} \tag{3}$$

In kinematic nonlinear systems analyzed by the FEM the general element local nonlinear strains $\boldsymbol{\varepsilon}$ consists of a membrane strain ε^{m} and a curvature $\boldsymbol{\kappa}$. This can be written in the general form, see e.g. [29]:

$$\boldsymbol{\varepsilon} = \begin{Bmatrix} \varepsilon^{\mathrm{m}} \\ \boldsymbol{\kappa} \end{Bmatrix} = \mathbf{B}\mathbf{v} + \frac{1}{2}\sum_{i=1}^{\mu} \mathbf{I}_i \mathbf{v}^T \mathbf{S}_i \mathbf{v} \tag{4}$$

where $\mathbf{v}$ represents the element DOFs, $\mathbf{B}$ is the matrix from a linear formulation, $\mathbf{S}_i$ is a symmetric matrix originating from nonlinear strain contributions and $\mathbf{I}_i$ is a column vector which places the i-th nonlinear term in the correct position. Furthermore, μ is the number of nonlinear strain terms included in $\boldsymbol{\varepsilon}^m$ and $\boldsymbol{\kappa}$. From the general strain formulation the element local internal restoring forces $\mathbf{g}_e(\mathbf{v})$ and tangent stiffness matrix $\mathbf{k}_T(\mathbf{v})$ can be written in the general form as

$$\mathbf{g}_e(\mathbf{v}) = \int_\Omega \left(\mathbf{B}^T\mathbf{D}\mathbf{B} + \frac{1}{2}\sum_{\ell=1}^{\mu}\sum_{m=1}^{\mu} \left(\mathbf{B}^T\mathbf{D}\mathbf{I}_m\mathbf{v}^T\mathbf{S}_m + 2\mathbf{S}_\ell\mathbf{v}\mathbf{I}_\ell\mathbf{D}\mathbf{B} + \mathbf{S}_\ell\mathbf{v}\mathbf{I}_\ell^T\mathbf{D}\mathbf{I}_m\mathbf{v}^T\mathbf{S}_m \right) \right)\mathbf{v}\, d\Omega \tag{5}$$

$$\mathbf{k}_T(\mathbf{v}) = \int_\Omega \mathbf{B}^T\mathbf{D}\mathbf{B} + \sum_{\ell=1}^{\mu}\sum_{m=1}^{\mu} \left[\mathbf{B}^T\mathbf{D}\mathbf{I}_m\mathbf{v}^T\mathbf{S}_m + \mathbf{S}_\ell\mathbf{v}\mathbf{I}_\ell^T\mathbf{D}\mathbf{B} + \mathbf{S}_\ell\mathbf{v}\mathbf{I}_\ell^T\mathbf{D}\mathbf{I}_m\mathbf{v}^T\mathbf{S}_m + \left| \mathbf{I}_\ell^T\mathbf{D}\mathbf{B}\mathbf{v} + \frac{1}{2}\mathbf{I}_\ell^T\mathbf{D}\mathbf{I}_m\mathbf{v}^T\mathbf{S}_m\mathbf{v} \right| \mathbf{S}_\ell \right] d\Omega \tag{6}$$

where Ω is the element domain, $\mathbf{D}$ is a stiffness matrix and $|()|$ indicates a scalar. The global internal restoring forces in (2) and the global tangent stiffness matrix in (3) are found by assembling all of the local element contributions in (5) and (6). In the following the above introduced general equations are exemplified by considering the plane Euler-Bernoulli beam element.

2.2. *The Euler-Bernoulli Beam*

Considering an Euler-Bernoulli beam, the governing equations of motion including the axial (membrane) strain, ε^{m}, and the curvature, κ, are given as, see e.g. [30];

$$\rho(x)\frac{\partial^2 w}{\partial t^2} + \frac{\partial^2}{\partial x^2}\left(EI(x)\kappa \right) = p(x) \tag{7}$$

$$\rho(x)\frac{\partial^2 u}{\partial t^2} - \frac{\partial}{\partial x}\left(EA(x)\varepsilon^{\mathrm{m}} \right) = q(x) \tag{8}$$

where x is the local beam co-ordinate, $w(x) = w$ and $u(x) = u$, respectively, are the transverse and the axial deformation along the un-deformed beam axis, $EI(x)$ is the bending stiffness, $EA(x)$ is the axial stiffness, $\rho(x)$ is the density per unit length, t is the time, and $p(x)$ and $q(x)$ represent the external loads in the transverse and axial beam directions, respectively. Damping is not included in (7) and (8) and will not be considered for the sake of simplicity. In addition, the beams considered are said to be homogeneous, i.e. $\rho(x) = \rho$, $EA(x) = EA$ and $EI(x) = EI$. Choosing a Lagrange-type strain measure, valid for moderate rotations, the element local strains are given as

$$\boldsymbol{\varepsilon} = \begin{Bmatrix} \varepsilon^{\mathrm{m}} \\ \kappa \end{Bmatrix} = \underbrace{\begin{Bmatrix} u' \\ w'' \end{Bmatrix}}_{\text{linear}} + \underbrace{\begin{Bmatrix} \frac{1}{2}(w')^2 \\ 0 \end{Bmatrix}}_{\text{nonlinear}} \tag{9}$$

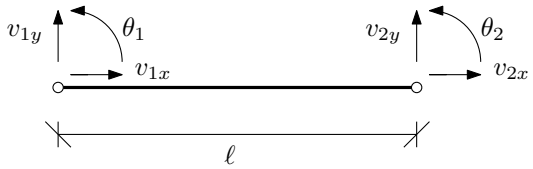

Figure 1. Plane Euler-Bernoulli beam element.

with the notation $()' = d()/dx$. The strain definitions in (9) is seen to introduce a nonlinear coupling between the governing EOMs in (7) and (8). This is referred to as a geometric second order effect.

In Figure 1 the plane Euler-Bernoulli beam element is shown. The element spans the domain Ω of length ℓ and has two nodes, each with two translational DOFs, v_{ix} and v_{iy}, and one rotational DOF, θ_i, i ϵ [1,2]. The DOFs are collected in the local element vector $\mathbf{v}$:

$$\mathbf{v} = \begin{bmatrix} v_{1x}, & v_{1y}, & \theta_1, & v_{2x}, & v_{2y}, & \theta_2 \end{bmatrix}^T \tag{10}$$

The displacements are interpolated as an interpolation matrix, $\mathbf{N}$, multiplied by the displacement vector $\mathbf{v}$:

$$\mathbf{u} = \begin{Bmatrix} u \\ w \end{Bmatrix} = \begin{bmatrix} \mathbf{N}_u \\ \mathbf{N}_w \end{bmatrix} \mathbf{v} = \mathbf{N}\mathbf{v} \tag{11}$$

In the given case $\mathbf{N}$ contains shape functions of first order used to describe the axial deformations and third order shape functions to describe the transverse deformations, see e.g. [31]. In order to establish the strains in (9) in discrete form, the following quantities are introduced:

$$u' = \mathbf{N}'_u\mathbf{v} = \mathbf{B}_\varepsilon\mathbf{v} \quad , \quad w' = \mathbf{N}'_w\mathbf{v} \quad , \quad w'' = \mathbf{N}''_w\mathbf{v} = \mathbf{B}_\kappa\mathbf{v} \tag{12}$$

With the quantities defined in (12), the general strains in (9) are formulated as:

$$\boldsymbol{\varepsilon} = \mathbf{B}\mathbf{v} + \frac{1}{2}\begin{Bmatrix} 1 \\ 0 \end{Bmatrix}\mathbf{v}^T\mathbf{G}\mathbf{v} \quad , \quad \mathbf{B} = \begin{Bmatrix} \mathbf{B}_\varepsilon \\ \mathbf{B}_\kappa \end{Bmatrix} \quad , \quad \mathbf{G} = \left(\mathbf{N}'_w\right)^T\mathbf{N}'_w \tag{13}$$

where $\mathbf{G}$ is a symmetric matrix. The strains in (13) represent the general formulation in (4) with $\mu = 1$, $\mathbf{I}_1 = \begin{bmatrix} 1 & 0 \end{bmatrix}^T$ and $\mathbf{S}_1 = \mathbf{G}$. The generalized stresses, $\boldsymbol{\sigma}$, consist of the normal force, N_σ, and the moment, M_σ. By assuming that the material is elastic, the constitutive relationship is given as:

$$\boldsymbol{\sigma} = \begin{Bmatrix} \mathrm{N}_\sigma \\ \mathrm{M}_\sigma \end{Bmatrix} = \mathbf{D}\boldsymbol{\varepsilon} \quad , \quad \mathbf{D} = \begin{bmatrix} EA & 0 \\ 0 & EI \end{bmatrix} \tag{14}$$

By use of the approximations in (11)-(14), the element local internal restoring forces in (5) become

$$\mathbf{g}_e(\mathbf{v}) = \int_\Omega \left(\mathbf{B}^T\mathbf{D}\mathbf{B} + \frac{EA}{2}\left(\mathbf{B}_\epsilon^T\mathbf{v}^T\mathbf{G} + 2\mathbf{G}\mathbf{v}\mathbf{B}_\epsilon + \mathbf{G}\mathbf{v}\mathbf{v}^T\mathbf{G}\right)\right)\mathbf{v}\, d\Omega \tag{15}$$

According to the definition in (2) the element local secant stiffness matrix can be identified from (15) as

$$\mathbf{k}_s(\mathbf{v}) = \int_\Omega \mathbf{B}^T\mathbf{D}\mathbf{B} + \frac{EA}{2}\left(\mathbf{B}_\epsilon^T\mathbf{v}^T\mathbf{G} + 2\mathbf{G}\mathbf{v}\mathbf{B}_\epsilon + \mathbf{G}\mathbf{v}\mathbf{v}^T\mathbf{G}\right)\, d\Omega \tag{16}$$

Furthermore, from the definition in (3) or from the generalization in (6) the element local tangent stiffness matrix is given as

$$\mathbf{k}_T(\mathbf{v}) = \int_\Omega \mathbf{B}^T\mathbf{D}\mathbf{B} + EA\left(\mathbf{B}_\varepsilon^T\mathbf{v}^T\mathbf{G} + \mathbf{G}\mathbf{v}\mathbf{B}_\varepsilon + \mathbf{G}\mathbf{v}\mathbf{v}^T\mathbf{G} + \mathbf{B}_\varepsilon\mathbf{v}\mathbf{G} + \frac{1}{2}\mathbf{v}^T\mathbf{G}\mathbf{v}\mathbf{G}\right)\, d\Omega \tag{17}$$

To obtain the global internal restoring forces, the global secant matrix and the global tangent stiffness matrix, all local element contributions in (15), (16) and (17) are assembled.

2.3. *Kinematic Nonlinear Behavior*

To illustrate the geometric second order coupling effect introduced through the strains in (9), a cantilever beam exposed to a static transverse deformation, $w(\ell, t)$, at the beam end ($x = \ell$) at time t, is sketched to the left in Figure 2.

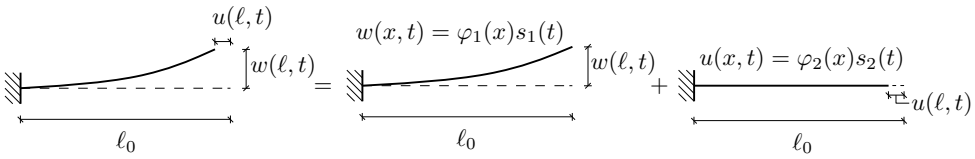

Figure 2. Kinematic Nonlinear Cantilever Beam.

Due to the coupling the transverse displacement $w(x, t)$ introduces a nonzero axial displacement $u(x, t)$ along the beam. This is realized by considering the axial strain measure in (9). If, for simplicity, it is assumed that the axial forces are negligible, the axial strains, ε, are zero throughout the beam, i.e.:

$$\varepsilon = \frac{\partial u}{\partial x} + \frac{1}{2}\left(\frac{\partial w}{\partial x}\right)^2 = 0 \tag{18}$$

The displacement $u(x, t)$ is then found by integrating the axial strain over the beam length. The integral is presented in (19) where the nonlinear coupling is seen to introduce a negative axial displacement of the beam, i.e. a beam contraction.

$$u(x,t) = -\frac{1}{2}\int_0^x \left(\frac{\partial w}{\partial x}\right)^2 dx \tag{19}$$

If the transverse displacement is changed to be dynamic, the time response could be analyzed by modal analysis (see Section 3). In this case the displacement of any point along the beam is considered as a sum of the transverse displacement $w(x, t)$ and the axial displacement $u(x, t)$, see Figure 2. Each of the displacement fields are then represented by two modes, referred to as $\varphi_1(x)$ and $\varphi_2(x)$, each multiplied by two time dependent scalar factors $s_1(t)$ and $s_2(t)$ to be determined. If only $w(x, t)$ is of interest and the system is linear it is sufficient to include the mode $\varphi_1(x)$ in the analysis and determine $s_1(t)$. However, in kinematic nonlinear analysis, where $w(x, t)$ and $u(x, t)$ couple, it is of crucial importance to also include the coupling activated deformation mode $\varphi_2(x)$ and its weight $s_2(t)$. Otherwise, the system may experience so-called membrane locking, in which the stiffness of the system is increased; see [32]. The possible consequences of locking are poorly predicted displacements and/or an unstable system. However, the basis vectors representing the nonlinear coupling effects may be difficult to pick, particularly for complex systems. Though, one way of representing the coupling activated basis vectors is by applying the MDs. This is illustrated in the following section by considering a Taylor series of the displacement vector $\mathbf{V}$ introduced in (1).

3. BASIS PROJECTION & MODAL DERIVATIVES

The number of DOFs n contained in the discretized EOMs in (1) can be reduced by projecting the latter onto a reduced subspace. This is done by introducing a relationship between the physical and the reduced subspace co-ordinates. For example a linear relation of the form

$$\mathbf{V}(\mathbf{s}) = \mathbf{\Phi}\mathbf{s} \tag{20}$$

where $\mathbf{\Phi}$ is an $n \times N$ basis matrix containing N basis vectors arranged as columns, where $N \leq n$. Furthermore, $\mathbf{s}$ is an $N \times 1$ vector containing the N reduced subspace co-ordinates, $s_i(t) = s_i$, which

are all functions of time. Inserting (20) into (1) and multiplying by $\mathbf{\Phi}^T$ on the left hand side, yields the general formulation for the projected nonlinear EOMs

$$\tilde{\mathbf{m}}\ddot{\mathbf{s}} + \tilde{\mathbf{c}}\dot{\mathbf{s}} + \tilde{\mathbf{g}}(\mathbf{s}) = \tilde{\mathbf{f}}(t) \tag{21}$$

where the following matrix definitions have been introduced

$$\tilde{\mathbf{m}} = \mathbf{\Phi}^T\mathbf{M}\mathbf{\Phi} \tag{22}$$

$$\tilde{\mathbf{c}} = \mathbf{\Phi}^T\mathbf{C}\mathbf{\Phi} \tag{23}$$

$$\tilde{\mathbf{g}}(\mathbf{s}) = \mathbf{\Phi}^T\mathbf{g}(\mathbf{\Phi}\mathbf{s}) \tag{24}$$

$$\tilde{\mathbf{f}}(t) = \mathbf{\Phi}^T\mathbf{F}(t) \tag{25}$$

The accuracy of the solution $\mathbf{V}(\mathbf{s})$ found by first solving the projected EOMs in (21) and then followed by a transformation of the $\mathbf{s}$ vector into physical co-ordinates by use of (20) depends on the basis vectors included in $\mathbf{\Phi}$. The lowest modes are usually always included. Furthermore, the basis vectors with a shape and frequency similar to the loading should be included to obtain a good approximate solution. Basis vectors representing the nonlinear coupling effects are also important as discussed in section 2.3. Typically, the number of reduced basis vectors required to obtain a good approximate solution from (21) is usually much smaller than the number of DOFs, that is, $N \ll n$. The size of the ratio N/n will, however, depend on the case considered.

3.1. Mode Shapes & Modal Derivatives

The system mode shapes $\boldsymbol{\varphi}_i$ are often included in the basis matrix $\mathbf{\Phi}$. They are also referred to as the *system mode shapes* or simply just as the *mode shapes*. The associated reduced co-ordinates s_j are referred to as the *modal co-ordinates*. The mode shapes fulfill the linearized eigenvalue problem

$$(\mathbf{K}_T(\mathbf{V}) - \omega_i^2\mathbf{M})\boldsymbol{\varphi}_i = \mathbf{0} \tag{26}$$

with ω_i denoting the corresponding natural angular frequencies. It is easy to identify which of the mode shapes that have a shape and frequency similar to the loading considered, and therefore should be included in the basis matrix. However, no guidelines to identify which of the mode shapes that represent the geometric second order effects exist. Instead, the MDs can be used to represent the second order effects. To realize this, the discrete displacement vector $\mathbf{V}(\mathbf{s})$ is expanded as a Taylor series in the modal co-ordinates s_j

$$\mathbf{V}(\mathbf{s}) = \mathbf{V}_0 + \sum_{j=1}^{N}\frac{\partial\mathbf{V}_0}{\partial s_j}(s_j - s_{j0}) + \frac{1}{2}\sum_{j=1}^{N}\sum_{k=1}^{N}\frac{\partial^2\mathbf{V}_0}{\partial s_j\partial s_k}(s_j - s_{j0})(s_k - s_{k0}) + \ldots \tag{27}$$

where the subscript 0 refers to the reference state. A basis formulation including N mode shape vectors and N modal co-ordinates is then introduced as

$$\mathbf{V}(\mathbf{s}) = \mathbf{\Phi}\mathbf{s} = \sum_{i=1}^{N}\boldsymbol{\varphi}_i s_i \tag{28}$$

The first and second order displacement derivatives in the Taylor series are then written in the form

$$\frac{\partial\mathbf{V}_0}{\partial s_j} = \frac{\partial}{\partial s_j}\left(\sum_{i=1}^{N}\boldsymbol{\varphi}_i s_i\right)_0 = \sum_{i=1}^{N}\frac{\partial\boldsymbol{\varphi}_{i0}}{\partial s_j}s_{i0} + \boldsymbol{\varphi}_{j0} \tag{29}$$

$$\frac{\partial^2\mathbf{V}_0}{\partial s_j\partial s_k} = \frac{\partial}{\partial s_k}\left(\frac{\partial\mathbf{V}_0}{\partial s_j}\right) = \sum_{i=1}^{N}\frac{\partial^2\boldsymbol{\varphi}_{i0}}{\partial s_j s_k}s_{i0} + \frac{\partial\boldsymbol{\varphi}_{k0}}{\partial s_j} + \frac{\partial\boldsymbol{\varphi}_{j0}}{\partial s_k} \tag{30}$$

From (29) and (30), the displacement derivatives are seen to include the mode shapes and their first and second order MDs. Thus, the MDs are seen to be of importance to the representation of

the higher order response. If, for simplicity, zero initial deformations ($s_{i0} = 0$) are considered, the Taylor series in (27) reduces to

$$\mathbf{V}(\mathbf{s}) = 0 + \sum_{j=1}^{N} \boldsymbol{\varphi}_{j0} s_j + \sum_{j=1}^{N} \sum_{k=1}^{j} \left(\frac{\partial \boldsymbol{\varphi}_{k0}}{\partial s_j} + \frac{\partial \boldsymbol{\varphi}_{j0}}{\partial s_k} \right) s_j s_k + ... \tag{31}$$

From (31) it is seen that the first order terms are represented solely by the N mode shapes, whereas the second order terms are represented solely by the N^2 MDs of first order. Thus, from the Taylor series it is seen that the MDs represent the coupling activated basis vectors. In the following two sets of equations governing the MDs are considered.

3.2. The Complete Governing System of Equations

In the following a novel set of equations governing the first order MDs is presented. The equations are referred to as *the complete governing system of equations* and they are based on perturbation methods. Only the main steps in the derivations are presented here. For details see Appendix A. The starting point of the derivations is to consider the free undamped kinematically nonlinear EOMs:

$$\mathbf{M}\ddot{\mathbf{V}} + \mathbf{g}(\mathbf{V}) = \mathbf{0} \tag{32}$$

A higher order displacement field and its corresponding acceleration field are introduced into (32). The Taylor series in (27) is taken as the natural choice to represent the displacement field. The acceleration is found by differentiating the Taylor series twice with respect to time:

$$\ddot{\mathbf{V}}(\mathbf{s}) = \sum_{j=1}^{N} \frac{\partial \mathbf{V}_0}{\partial s_j} \ddot{s}_j + \frac{1}{2} \sum_{j=1}^{N} \sum_{k=1}^{N} \frac{\partial^2 \mathbf{V}_0}{\partial s_j \partial s_k} \left[\ddot{s}_j (s_k - s_{k0}) + 2\dot{s}_j \dot{s}_k + (s_j - s_{j0}) \ddot{s}_k \right] + ... \tag{33}$$

It is then assumed that the co-ordinates s_j are given in a complex form similar to a linear harmonic solution

$$s_j = A_j e^{i\omega_j(\mathbf{s})t} + s_{j0} \tag{34}$$

with A_j denoting the amplitude. This is multiplied by the complex exponential function dependent on the time, t, and the frequency $\omega_j(\mathbf{s})$. Furthermore, s_{j0} represents an offset from zero. As the free and undamped system is considered the amplitude is assumed to be constant. The frequency, however, will be a function of the displacement field since kinematic nonlinearities are included. This is formulated as a Taylor series:

$$\omega_j(\mathbf{s}) = \omega_{j0} + \sum_{k=1}^{N} \frac{\partial \omega_{j0}}{\partial s_k} (s_k - s_{k0}) + ... \tag{35}$$

Differentiating (34) with respect to time the velocity and acceleration in modal co-ordinates are evaluated as:

$$\dot{s}_j(t) = i(\omega_j(\mathbf{s}) + \dot{\omega}_j(\mathbf{s})t)(s_j - s_{j0}) \tag{36}$$

$$\ddot{s}_j(t) = \left[i\left(\ddot{\omega}_j(\mathbf{s})t + 2\dot{\omega}_j(\mathbf{s})\right) - \left(\dot{\omega}_j(\mathbf{s})t + \omega_j(\mathbf{s})\right)^2 \right] (s_j - s_{j0}) \tag{37}$$

By introducing (27) and (33) - (37) into (32), the latter is expressed as a polynomial in the modal co-ordinates of the form:

$$\mathbf{A} + \sum_{j=1}^{N} \mathbf{B}_j s_j + \sum_{j=1}^{N} \sum_{k=1}^{N} \mathbf{C}_{jk} s_j s_k + ... = \mathbf{0} \tag{38}$$

where $\mathbf{A}$, $\mathbf{B}_j$ and $\mathbf{C}_{jk}$ in (38) are the zero, first and second order vector coefficients, respectively. Since the co-ordinates s_j can take on any value, it can be argued that all of the vector coefficients should be zero in order for the equations to be satisfied in all cases, i.e.:

$$\mathbf{A} = \mathbf{0} \tag{39}$$

$$\mathbf{B}_j = \mathbf{0} \tag{40}$$

$$\mathbf{C}_{jk} = \mathbf{0} \tag{41}$$

Each of the equations in (39)-(41) yield a set of governing equations. The equations including the zero order coefficient in (39) represent the EOMs; the equations including the first order coefficients in (40) represent the eigenvalue problem; and the equations including the second order coefficients in (41) represent the equations governing the first and second order MDs.

In Appendix A the equations in (41) are derived in general form with $s_{j0} = 0$. The reason for introducing the zero displacement condition is that it eliminates the second order MDs from the equations. Thus, for $s_{j0} = 0$ the equations in (41) only govern the desired first order MDs considered in the present work. The governing equations are expressed as

$$\left[\mathbf{K}_T(\mathbf{0}) - (\omega_{j0} + \omega_{k0})^2\mathbf{M}\right]\frac{1}{2}\left(\frac{\partial \boldsymbol{\varphi}_{k0}}{\partial s_j} + \frac{\partial \boldsymbol{\varphi}_{j0}}{\partial s_k}\right) = \left[\alpha_0\mathbf{M} - \frac{\partial \mathbf{K}_S(\mathbf{0})}{\partial s_k}\right]\boldsymbol{\varphi}_{j0} \tag{42}$$

with the subscript 0 indicating the zero displacement reference state. In (42) the MDs of first order appear as a sum on the left hand side. The sum of these are easily determined by inverting the matrix $[\mathbf{K}_T(\mathbf{0}) - (\omega_{j0} + \omega_{k0})^2\mathbf{M}]$, consisting of the difference between the tangent stiffness and the mass matrix multiplied by the squared sum of the linear natural frequencies. The right hand side consists of the mass matrix multiplied by a coefficient denoted α_0. The differentiated secant stiffness is subtracted from this, before multiplying by the j-th mode shape. The coefficient α_0 is given as a function of the mass matrix, the mode shapes j and k and the secant stiffness matrix differentiated with respect to j and k, respectively:

$$\alpha_0 = \frac{\boldsymbol{\varphi}_{j0}^T}{\boldsymbol{\varphi}_{j0}^T\mathbf{M}\boldsymbol{\varphi}_{j0}}\left(\frac{\partial \mathbf{K}_S(\mathbf{0})}{\partial s_k}\boldsymbol{\varphi}_{j0} - \frac{\partial \mathbf{K}_S(\mathbf{0})}{\partial s_j}\boldsymbol{\varphi}_{k0}\right) \tag{43}$$

An example of the formulation of the differentiated secant stiffness matrices in (43) is given in Appendix B considering the Euler-Bernoulli beam element.

The equations in (42) constitute the complete governing system of equations for the MDs of first order in the case of zero initial displacements. In the following the first order MDs determined from this system of equations are referred to as *the complete MDs*. It is, however, important to stress that the complete MDs can only be determined as a sum of two vectors from (42). A compact formulation for this solution is introduced as

$$\partial\boldsymbol{\varphi}_{kj} = \frac{\partial \boldsymbol{\varphi}_k}{\partial s_j} + (1 - \delta_{kj})\frac{\partial \boldsymbol{\varphi}_j}{\partial s_k} \quad , \quad k, j \,\epsilon\, [1; N] \;\wedge\; j \leq k \tag{44}$$

where N is the number of mode shapes in the Taylor series of $\mathbf{V}(\mathbf{s})$, and δ_{kj} represents the Kronecker delta. Given N mode shapes, then there are $H = \frac{1}{2}(N + N^2)$ combinations of $\partial\boldsymbol{\varphi}_{kj}$.

3.3. Differentiated Eigenvalue Problem Including Geometric Restriction

In the present subsection the singular system of equations governing the first order MDs introduced in [18, 23] are considered. In the following it is shown how the singularity can be removed by introducing a novel geometric restriction.

The singular governing system of equations is derived from the linearized eigenvalue problem in (26) in differentiated form, cf. [18, 23]. If the derivative of the mode shape $\boldsymbol{\varphi}_k$ with respect to the j-th modal co-ordinate is required, then the eigenvalue problem in (26) is differentiated with respect to s_j. This leads to the system of first order differential equations:

$$\left(\mathbf{K}_T(\mathbf{V}) - \omega_k^2\mathbf{M}\right)\frac{\partial \boldsymbol{\varphi}_k}{\partial s_j} = \left(\frac{\partial \omega_k^2}{\partial s_j}\mathbf{M} - \frac{\partial \mathbf{K}_T(\mathbf{V})}{\partial s_j}\right)\boldsymbol{\varphi}_k \tag{45}$$

The desired first order MD is seen to appear on the left hand side, multiplied by the matrix appearing in the eigenvalue problem in (26). The right hand side consists of a matrix, which is the difference between the product of the squared natural frequency in differentiated form and the mass matrix, and the tangent stiffness in differentiated form. This matrix is multiplied by the k-th mode shape.

Several significant differences are observed when (45) is compared with (42). First of all, it is the tangent stiffness that appears on the right hand side of the approximate equations in (45), whereas the secant stiffness appears in the complete governing system of equations in (42). Furthermore, on the left hand side of (45), only a single modal derivative and its corresponding natural frequency appear, whereas in (42) the complete MDs appear as a sum of vectors, and the corresponding natural frequencies appear as a squared sum.

The reason for the significant differences between the two governing system of equations is that the equations in (45) are based on the linearized eigenvalue problem. When a linearized set of equations are differentiated, the result will only represent an approximation of the actual derivative. Thus, the equations in (45) represent an approximation of the complete governing system of equations in (42). This is illustrated by way of an example in Section 4.

As the matrix on the left hand side of (45) appears in the eigenvalue problem in (26) the system of equations is by default known to be singular. Thus, it is not possible to invert the matrix and determine the modal derivative from the system of equations in (45). However, by introducing a geometric restriction on the MDs it is possible to eliminate the singularity.

The full solution to the modal derivative in (45) is given as a sum of the homogeneous solution and a particular solution

$$\frac{\partial \boldsymbol{\varphi}_k}{\partial s_j} = \left\{ \frac{\partial \boldsymbol{\varphi}_k}{\partial s_j} \right\}_{Hom} + \left\{ \frac{\partial \boldsymbol{\varphi}_k}{\partial s_j} \right\}_{Part} \quad , \quad \left\{ \frac{\partial \boldsymbol{\varphi}_k}{\partial s_j} \right\}_{Hom} = \beta \boldsymbol{\varphi}_k \tag{46}$$

Since the matrix on the left hand side of (45) is identical to the matrix in the eigenvalue problem in (26) the homogenous solution is given as the k-th mode shape times an arbitrary scalar β.

A geometric restriction could be to demand that the homogenous and the particular solutions are orthogonal, i.e. that their scalar product is zero. An argument in support of this is that if the particular solution includes information already present in the homogenous solution, this information would be redundant, and vice versa. Thus, a geometric restriction may be expressed as:

$$\left\{ \frac{\partial \boldsymbol{\varphi}_k}{\partial s_j} \right\}_{Hom}^T \left\{ \frac{\partial \boldsymbol{\varphi}_k}{\partial s_j} \right\}_{Part} = 0 \tag{47}$$

Assuming the particular MD to have a frequency different from the homogenous MD, the mass and stiffness orthogonality conditions known from linear theory also apply, i.e.:

$$\boldsymbol{\varphi}_k^T \mathbf{K}_T(\mathbf{V}) \left\{ \frac{\partial \boldsymbol{\varphi}_k}{\partial s_j} \right\}_{Part} = 0 \tag{48}$$

$$\boldsymbol{\varphi}_k^T \mathbf{M} \left\{ \frac{\partial \boldsymbol{\varphi}_k}{\partial s_j} \right\}_{Part} = 0 \tag{49}$$

Considering the governing system of equations in (45) to be derived from a minimization condition with the MD as the variable parameter, the Lagrange multiplier method can be applied to introduce a geometric condition, see for example [32]. Introducing the condition in (47) together with the definition in (46) into (45) the following system of equations is found:

$$\begin{bmatrix} \left(\mathbf{K}_T(\mathbf{V}) - \omega_k^2 \mathbf{M}\right) & \boldsymbol{\varphi}_k \\ \boldsymbol{\varphi}_k^T & 0 \end{bmatrix} \begin{Bmatrix} \left\{ \frac{\partial \boldsymbol{\varphi}_k}{\partial s_j} \right\}_{Part} \\ \lambda \end{Bmatrix} = \begin{Bmatrix} \left(\frac{\partial \omega_k^2}{\partial s_j} \mathbf{M} - \frac{\partial \mathbf{K}_T(\mathbf{V})}{\partial s_j} \right) \boldsymbol{\varphi}_k \\ 0 \end{Bmatrix} \tag{50}$$

with λ being the Lagrange multiplier, which is an additional unknown. In the present case, this is a scalar. The governing system of equations in (50) is non-singular and is referred to as *the*

approximate governing system of equations in the following. Furthermore, the first order MDs determined from the equations are referred to as *the approximate MDs*.

It should be stressed that, due to the introduction of the geometric condition in (47), the MD in (50) only represents the particular solution. To obtain the full MD, this must be added to the homogenous solution in (46). However, in order to avoid singularity issues in a basis including both mode shapes and MDs $\beta = 0$ is selected. Thus, the MDs only consist of the particular parts.

The differentiated natural frequency in (50) is found by multiplying (45) by $\boldsymbol{\varphi}_k^T$ and apply the relations in (48) - (49). This is shown in [27] and yields the expression:

$$\frac{\partial \omega_k^2}{\partial s_j} = \frac{\boldsymbol{\varphi}_k^T}{\boldsymbol{\varphi}_k^T \mathbf{M} \boldsymbol{\varphi}_k} \frac{\partial \mathbf{K}_T(\mathbf{V})}{\partial s_j} \boldsymbol{\varphi}_k \tag{51}$$

From (51) the differentiated frequency is seen to be a function of the k-th mode shape, the mass matrix and the differentiated tangent stiffness matrix.

4. ILLUSTRATIVE EXAMPLE - HIGHLY NONLINEAR CABLE

In this section the differences between using the complete MDs and the approximate MDs in a basis projection are studied. For this the response of a highly nonlinear simply supported cable, modeled by Euler-Bernoulli elements and exposed to harmonic loading, is analyzed.

Firstly, a description of the cable example under consideration, including geometry, stiffness parameters, and loading is given. Next it is illustrated that the cable displays sufficient nonlinear behavior to represent a relevant study case. Finally, an analysis and a discussion of the displacement responses achieved with the complete MDs and the approximate MDs, respectively, are presented.

4.1. Cable Geometry and Loading

To demonstrate the precision of the complete and approximate MDs a simply supported highly nonlinear cable of length ℓ exposed to a transversely directed uniform load $p(t)$ along half of its length is considered, see Figure 3.

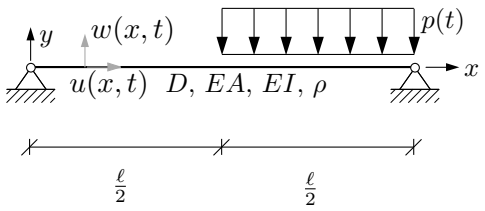

Figure 3. Simple supported kinematic nonlinear cable.

The cable has a diameter, D, a Young's modulus, E, a cross-sectional area, A, a second moment of area, I, and a density, ρ. The axial and transverse displacements are denoted $u(x,t)$ and $w(x,t)$, respectively. The load, $p(t)$, consists of two harmonic load contributions in phase with the first and second natural angular bending frequencies ω_1 and ω_2, respectively. Mathematically the load is expressed as:

$$p(t) = F_1 sin(\omega_1 t) + F_2 sin(\omega_2 t) \tag{52}$$

where F_1 and F_2 denote the load amplitudes. Table I presents the applied cable and load parameters.

4.2. Case Validation

In the following it is demonstrated that the cable example displays sufficient nonlinear behavior to be considered a relevant case study for kinematic nonlinearities. To simulate the response of the cable the implicit Newmark integration method and the explicit central difference method (CDM) are used. The parameters of the former correspond to the *average acceleration* case, see e.g. [33]. The algorithms are implemented into a local MATLAB-based FEM program.

Table I. Cable parameters.

Parameter	Unit	Formula	Magnitude
ℓ	m	-	20
E	GPa	-	210
D	mm	-	50
A	cm^2	$\pi\frac{D^2}{4}$	20
I	cm^4	$\pi\frac{D^4}{64}$	30.7
F_1	N/m	-	-1
F_2	N/m	-	-3
ρ	kg/m	-	15.6
ω_1	rad/s	$\left(\frac{\pi}{l}\right)^2\sqrt{EI/\rho}$	1.6
ω_2	rad/s	$\left(\frac{2\pi}{l}\right)^2\sqrt{EI/\rho}$	6.4

In Figure 4 a ten-second interval showing the linear and nonlinear transverse displacements of the cable midpoint, $w_m(t) = w(\ell/2, t)$ is plotted. This is done using the linear Newmark (LN), the nonlinear Newmark (NN), the linear CDM (LC) and the nonlinear CDM (NC) schemes, respectively. The responses represent the full solutions in the converged state with respect to both time step magnitude ($\Delta t = 10$ ms), iteration residual and the number of elements. To converge, the MATLAB models required 20 elements. Furthermore, a linear ABAQUS (LA) and a nonlinear ABAQUS (NA) solution including 30 elements are plotted. For the ABAQUS simulation a three-dimensional beam element with two nodes named B31 is used.

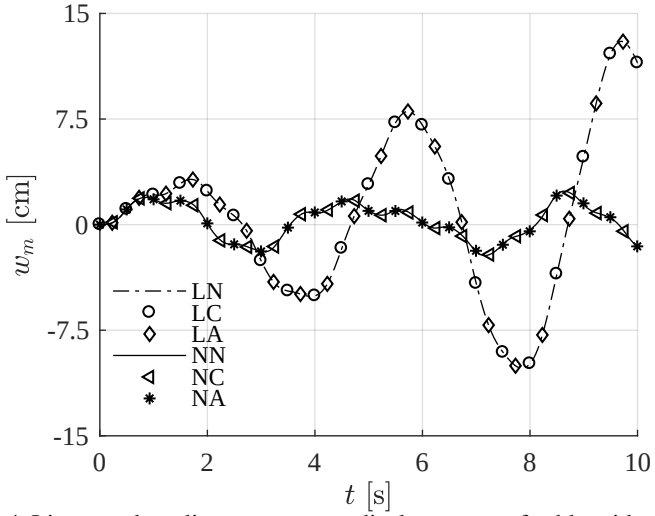

Figure 4. Linear and nonlinear transverse displacements of cable midpoint.

From the graph it is seen that all of the linear solutions are more or less identical. The same is true for all of the nonlinear solutions. This confirms the implementation of the applied MATLAB based algorithms to be correct. In the nonlinear case, the amplitude is seen to be more or less bounded; whereas, in the linear case the amplitude continues to increase during the entire time interval considered. The significantly different behavior in the linear and the nonlinear cases confirms that the structure is a relevant study case for kinematic nonlinearities.

4.3. Basis Analysis of Nonlinear Cable

In the following the nonlinear cable response is evaluated by use of basis projecting including mode shapes and MDs as basis vectors. The purpose of the analysis is to compare the solutions when including either the complete MDs or the approximate MDs as the first order modes in the basis. The FEM model contains 20 elements, corresponding to the element number in the converged

stage. Furthermore, all of the simulation results presented in the following are found by use of the CDM.

In Figure 5 the first $N = 3$ cable mode shapes and their $H = 6$ associated MDs are plotted as a function of the relative coordinate x/ℓ. To be able to compare directly the MDs determined from (42) and (50) the definition in (44) is applied.

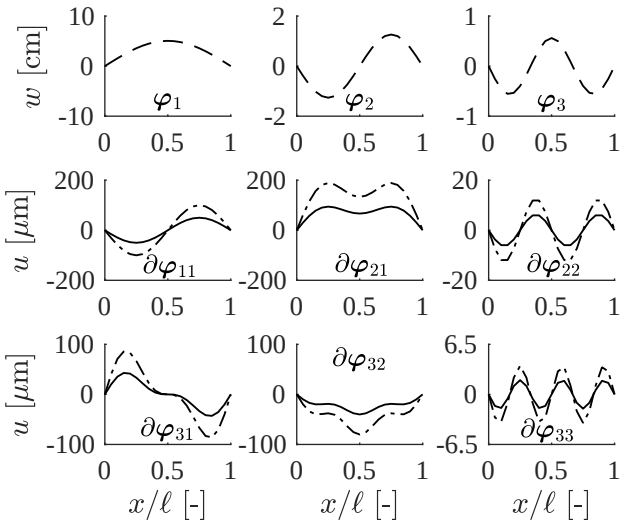

Figure 5. The cable mode shapes (- -), the complete MDs (–) and the approximate MDs (-·-).

The dashed lines in Figure 5 represent the mode shapes, the solid lines represent the complete MDs and the dashed-dotted lines represent the approximate MDs. The three mode shapes only represent bending (transverse) displacements, $w(x)$, whereas all of the MDs only represent axial displacements, $u(x)$. The mode shapes are formed as a number of harmonic half waves equal to the index number with zero displacements at the boundaries as a consequence of the introduced supports. The MDs are also seen to comply with the zero displacement boundary conditions. Furthermore, the MDs with indices $j = k$ are formed as $2k$ harmonic half waves, whereas no general trend with respect to shape is visible for the MDs with indices $k \neq j$. Instead, the latter can be described as continuous functions with an alternating number of local extrema. The complete MDs and the approximate MDs are seen to be more or less identical with respect to shape, but with an amplitude ratio of two. Moreover, the magnitudes of the MDs are seen to be relatively small compared to the mode shape amplitudes. From a Gauss elimination it was furthermore detected that a linear relation between the three MDs $\partial\boldsymbol{\varphi}_{22}$, $\partial\boldsymbol{\varphi}_{31}$ and $\partial\boldsymbol{\varphi}_{11}$ exist:

$$\partial\boldsymbol{\varphi}_{22} = -\frac{3}{8}\partial\boldsymbol{\varphi}_{31} - \frac{1}{4}\partial\boldsymbol{\varphi}_{11} \tag{53}$$

The linear relation in (53) entails that at least one of the three vectors has to be left out when analyzing the cable response by use of basis projection in order to avoid singularities.

Three different bases are used in the cable analysis with the basis matrices referred to as $\boldsymbol{\Phi}_i$, $i \in$ [1,3]. They contain the basis vectors marked by checkmarks (✓) in Table II.

Table II. Basis vectors included in basis analysis of the cable.

	$\boldsymbol{\varphi}_1$	$\boldsymbol{\varphi}_2$	$\boldsymbol{\varphi}_3$	$\partial\boldsymbol{\varphi}_{11}$	$\partial\boldsymbol{\varphi}_{21}$	$\partial\boldsymbol{\varphi}_{22}$	$\partial\boldsymbol{\varphi}_{31}$	$\partial\boldsymbol{\varphi}_{32}$	$\partial\boldsymbol{\varphi}_{33}$
$\boldsymbol{\Phi}_1$	✓	✓							
$\boldsymbol{\Phi}_2$	✓	✓		✓	✓	✓			
$\boldsymbol{\Phi}_3$	✓	✓	✓	✓	✓		✓	✓	✓

The first basis matrix $\mathbf{\Phi}_1$ consists of the first two mode shapes. The second basis matrix $\mathbf{\Phi}_2$ includes the first two mode shapes and their associated MDs defined in (44). The third basis matrix $\mathbf{\Phi}_3$ contains the first three mode shapes and all of the associated MDs, except from the linear dependent vector $\partial\boldsymbol{\varphi}_{22}$. Each of the three basis matrices applied in the analyses follow the linear basis concept introduced in (20), i.e. with an independent modal co-ordinate associated with each included basis vector. This implies that the displacement field approximated by the basis $\mathbf{\Phi}_3$ is written in mathematical form as:

$$\mathbf{V} = \underbrace{\begin{bmatrix}\boldsymbol{\varphi}_1 & \boldsymbol{\varphi}_2 & \boldsymbol{\varphi}_3 & \partial\boldsymbol{\varphi}_{11} & \partial\boldsymbol{\varphi}_{21} & \partial\boldsymbol{\varphi}_{31} & \partial\boldsymbol{\varphi}_{32} & \partial\boldsymbol{\varphi}_{33}\end{bmatrix}}_{\mathbf{\Phi}_3} \begin{Bmatrix} s_1 \\ s_2 \\ s_3 \\ s_4 \\ s_5 \\ s_6 \\ s_7 \\ s_8 \end{Bmatrix} \tag{54}$$

with the basis matrix $\mathbf{\Phi}_3$ containing the three mode shapes in the first three places and the MDs in the final places. The basis matrix is multiplied by a vector containing eight independent modal co-ordinates, where s_j, $j \in$ [1,3] belongs to the mode shapes and s_j, $j \in$ [4,8], belongs to the MDs.

Figure 6 shows the transverse displacement in the cable midpoint, $w_m(t)$, using the three basis approximations listed in Table II with the complete MDs selected to represent the first order modes. The basis responses are referred to as $\mathbf{\Phi}_i$, $i \in$ [1;3]. Also the converged NC curve from Figure 4 is plotted and used as reference. Figure 6a shows a 10-seconds time interval and Figure 6b shows a close-up.

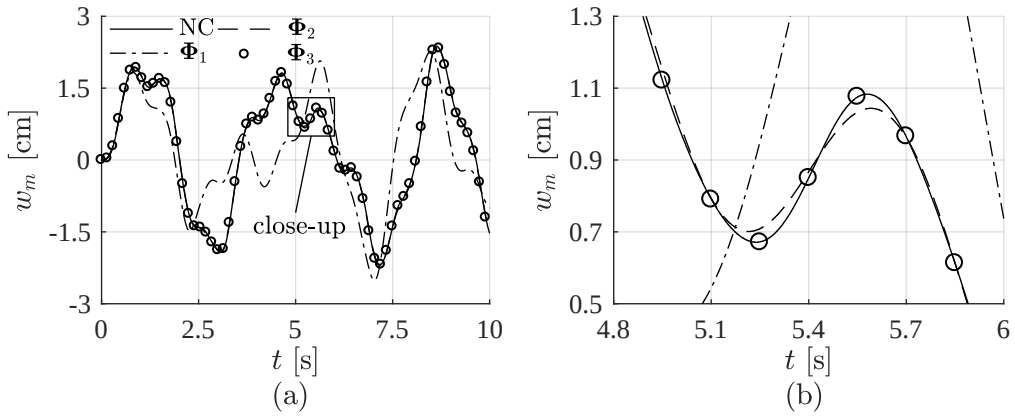

Figure 6. Transverse displacement of cable midpoint, $w_m(t)$, found by use of basis projection including the complete MDs considering (a) a 10 seconds interval and (b) a close-up.

From the plots in Figure 6, it is observed that the $\mathbf{\Phi}_1$ curve is significantly different from the NC solution. The amplitude is within the same order of magnitude, but the response frequency and shape are different. The response is greatly improved by adding the associated MDs. This is observed by considering the $\mathbf{\Phi}_2$ curve, which is almost identical to that of the full nonlinear NC solution, except for small deviations close to the local extrema, as seen in Figure 6b. By including the third mode shape and the associated MDs, the response curve becomes more or less identical to the NC solution, illustrated by the $\mathbf{\Phi}_3$ curve.

Identical results to the ones shown in Figure 6 are found when replacing the complete MDs with the approximate MDs in the basis formulations (not shown here). Based on these observations it is not possible to conclude if the complete MDs are better or more exact than the approximate MDs. In order to do so the modal co-ordinates from the cable example simulated with the basis in (54)

are considered. By inserting the linear relation in (53) into the Taylor series in (31) a set of relations between the modal co-ordinates s_j, $j \in$ [4,8] belonging to the MDs and the three modal co-ordinates s_j, $j \in$ [1,3] of the mode shapes are predicted to be:

$$s_4 = s_1^2 - \frac{1}{4}s_2^2 \tag{55}$$

$$s_5 = s_1 s_2 \tag{56}$$

$$s_6 = s_1 s_3 - \frac{3}{8}s_2^2 \tag{57}$$

$$s_7 = s_2 s_3 \tag{58}$$

$$s_8 = s_3^2 \tag{59}$$

The Taylor prediction in (55) states that the s_4 co-ordinate is equal to the term s_1^2 - $\frac{1}{4}s_2^2$. In Figure 7a this relation is plotted based on the co-ordinates obtained using the complete MDs, and in Figure 7b the relation is plotted based on the co-ordinates found using the approximate MDs.

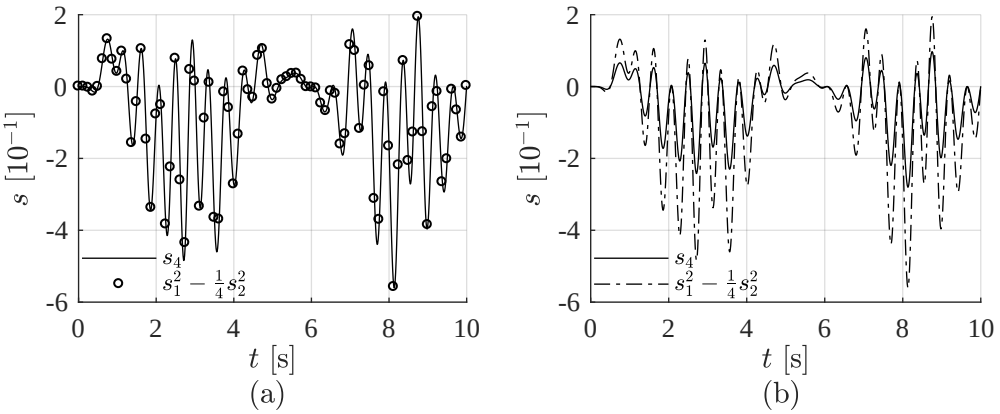

Figure 7. Plot of the modal co-ordinates s_4 and $s_1^2 - \frac{1}{4}s_2^2$ based on two modal analyzes including respectively (a) the complete MDs and (b) the approximate MDs.

From Figure 7a it is seen that the modal co-ordinates fulfill the prediction when the complete MDs are applied, as the plotted curves are identical. However, when the approximate MDs are used, the shapes of the two plotted curves are alike, but they differ by a factor of two, see Figure 7b. The same pattern appears when the remaining relationships in (56)-(59) are plotted (not shown here); that the co-ordinates associated with the complete MDs fulfill the predictions in (56)-(59), whereas the co-ordinates of the approximate MDs do not. From these observations it is concluded that the complete governing system of equations in (42) are seen to fulfill the Taylor series, whereas the approximate governing system of equations in (50) do not. Therefore, the complete governing system of equations in (42) are consistent with the Taylor series.

From the Taylor series in (27), it is possible to organize a basis where the co-ordinates of the MDs are known. This is referred to as a Taylor Basis. In this way the complete MDs can be included without increasing the number of unknowns (modal co-ordinates) in the system. In Paper II a basis taking into account this advantage is organized including the complete MDs and it is shown that the formulation can improve the computational efficiency and stability significantly.

5. CONCLUSION

Two novel systems of equations governing the first order modal derivatives have been derived. One was found by inserting a Taylor series for the displacement field into the free undamped

kinematic nonlinear equations of motion, and arguing that all coefficients should be zero to fulfill the system of equations. This was referred to as the complete governing system of equations. The second one was referred to as the approximate governing system of equations and it was found by introducing a novel geometric restriction into the differentiated eigenvalue problem. The response of a highly nonlinear cable exposed to harmonic loading was analysed by use of basis projecting including the system mode shapes and the first order modal derivatives. The example showed that the modal derivatives determined from the two novel governing systems of equations produced identical response solutions. However, only the modal derivatives determined from the complete governing system of equations fulfilled the Taylor series prediction. Based on these observations the complete governing system of equations was concluded to be consistent with the Taylor series.

A. DERIVATION OF THE COMPLETE GOVERNING SYSTEM OF EQUATIONS

The complete governing system of equations including the first order MDs are derived by use of perturbation methods. The starting point is the free undamped kinematic nonlinear EOMs

$$\mathbf{M}\ddot{\mathbf{V}} + \mathbf{g}(\mathbf{V}) = \mathbf{0} \tag{60}$$

with the internal restoring forces $\mathbf{g}(\mathbf{V})$ defined in (5) for a single element. The EOMs in (60) are expanded by introducing a Taylor series for the displacement field, $\mathbf{V}(\mathbf{s})$, and its acceleration, $\ddot{\mathbf{V}}(\mathbf{s})$, both expressed as a function of the modal co-ordinates collected in the vector $\mathbf{s}$. The displacement field is expressed as

$$\mathbf{V}(\mathbf{s}) = \mathbf{V}_0 + \sum_{j=1}^{N} \frac{\partial \mathbf{V}_0}{\partial s_j}(s_j - s_{j0}) + \frac{1}{2}\sum_{j=1}^{N}\sum_{k=1}^{N} \frac{\partial^2 \mathbf{V}_0}{\partial s_j \partial s_k}(s_j - s_{j0})(s_k - s_{k0}) + ... \tag{61}$$

with the subindex 0 referring to the reference stage. From equation (61) the acceleration is found by differentiating twice with respect to time t:

$$\ddot{\mathbf{V}}(\mathbf{s}) = \sum_{j=1}^{N} \frac{\partial \mathbf{V}_0}{\partial s_j}\ddot{s}_j + \sum_{j=1}^{N}\sum_{k=1}^{N} \frac{1}{2}\frac{\partial^2 \mathbf{V}_0}{\partial s_j \partial s_k}\left[\ddot{s}_j(s_k - s_{k0}) + 2\dot{s}_j\dot{s}_k + (s_j - s_{j0})\ddot{s}_k\right] + ... \tag{62}$$

with the time derivative denoted $\dot{()} = \partial()/\partial t$. The first and second order displacement derivatives in equation (61) and (62) include the first order modal derivatives of interest (see equation (29) and (30)). However, the equations also include to the second order modal derivatives which are not of interest in the present work. In order to remove these zero initial displacements are considered in the following derivations, i.e. $s_{i0} = 0 \; \epsilon \; [1; N]$. By this the displacement derivatives are reduced to

$$\left.\frac{\partial \mathbf{V}_0}{\partial s_j}\right|_{s_{i0}=0} = \boldsymbol{\varphi}_{j0} \tag{63}$$

$$\left.\frac{\partial^2 \mathbf{V}_0}{\partial s_j \partial s_k}\right|_{s_{i0}=0} = \frac{\partial \boldsymbol{\varphi}_{k0}}{\partial s_j} + \frac{\partial \boldsymbol{\varphi}_{j0}}{\partial s_k} \tag{64}$$

For zero initial displacements only the second order displacement derivative in (64) contains the first order modal derivatives of interest. Thus, this term is of key interest in the derivations. It is then assumed that the solution to the modal co-ordinates is given as:

$$s_j \equiv s_j(t) = A_j e^{i\omega_j(\mathbf{s})t} + s_{j0} \quad , \quad j \; \epsilon \left[1; N\right] \tag{65}$$

with A_j denoting the amplitude, s_{j0} representing an offset from zero and $\omega_j(\mathbf{s})$ denoting the associated frequency. When the free and undamped EOMs are considered, the amplitude is assumed to be constant. As kinematic nonlinearities are included, the stiffness, and thus also the natural frequency, will be dependent on the displacements represented by the modal co-ordinates $\mathbf{s}$.

Before the displacement and acceleration in (61) and (62) are inserted into the nonlinear EOMs in (60), the first and second order modal time derivatives, $\dot{s}_j$ and $\ddot{s}_j$, are expressed as a function of the non differentiated modal co-ordinates, s_j. From (65), the modal velocity and acceleration are found by differentiation as

$$\dot{s}_j(t) = i(\omega_j(\mathbf{s}) + \dot{\omega}_j(\mathbf{s})t)(s_j - s_{j0}) \tag{66}$$

$$\ddot{s}_j(t) = \left[i\left(\ddot{\omega}_j(\mathbf{s})t + 2\dot{\omega}_j(\mathbf{s})\right) - \left(\dot{\omega}_j(\mathbf{s})t + \omega_j(\mathbf{s})\right)^2\right](s_j - s_{j0}) \tag{67}$$

The derivations of the equations governing the MDs are for simplicity considered at time $t = 0$. This implies that the modal velocity and acceleration in (66) and (67) reduce to

$$\dot{s}_j \equiv \dot{s}_j(0) = i\omega_j(\mathbf{s})(s_j - s_{j0}) \tag{68}$$

$$\ddot{s}_j \equiv \ddot{s}_j(0) = \left[i2\dot{\omega}_j(\mathbf{s}) - \omega_j^2(\mathbf{s})\right](s_j - s_{j0}) \tag{69}$$

The modal velocity and acceleration in (68) and (69) are functions of the frequency and its first order time derivative. The frequency is expanded as a Taylor series in the modal co-ordinates

$$\omega_j(\mathbf{s}) = \omega_{j0} + \sum_{l=1}^{N} \frac{\partial \omega_{j0}}{\partial s_l}(s_l - s_{l0}) + \ldots \tag{70}$$

The time derivative of the frequency is expressed in the general form

$$\dot{\omega}_j(\mathbf{s}) = \sum_{r=1}^{N} \frac{\partial \omega_j(\mathbf{s})}{\partial s_r}\dot{s}_r \tag{71}$$

Inserting the Taylor series in (70) together with (68) into the first order time derivative of the natural frequency in (71), the latter can be written in the form:

$$\dot{\omega}_j(\mathbf{s}) = i\sum_{r=1}^{N}\left(\frac{\partial \omega_{j0}}{\partial s_r}\omega_{r0} + \ldots\right)(s_r - s_{r0}) \tag{72}$$

By use of (70) and (72) the modal velocity and acceleration in (68) and (69) can now be expressed as a function of the non differentiated modal co-ordinates. Inserting Equations (68)-(70) and Equation (72) into the acceleration in (62) for $s_{j0} = 0$, the latter can be expressed in the form

$$\ddot{\mathbf{V}}(\mathbf{s}) = .. - \sum_{j=1}^{N}\sum_{k=1}^{N}\left[2\boldsymbol{\varphi}_{j0}\frac{\partial \omega_{j0}}{\partial s_k}(\omega_{k0} + \omega_{j0}) + \frac{1}{2}\left(\frac{\partial \boldsymbol{\varphi}_{k0}}{\partial s_j} + \frac{\partial \boldsymbol{\varphi}_{j0}}{\partial s_k}\right)(\omega_{j0} + \omega_{k0})^2\right]s_j s_k + .. \tag{73}$$

Next, the Taylor series for the displacement field in (61) is inserted into the general expression for the global internal restoring forces $\mathbf{g}(\mathbf{V})$ (given as the definition in (5) with $\mathbf{v}$ replaced by $\mathbf{V}$). For $s_{j0} = 0$ and with (64) inserted this can be written as

$$\begin{aligned}\mathbf{g}(\mathbf{V}) = ..+\sum_{j=1}^{N}\sum_{k=1}^{N}\Bigg[&\underbrace{\int_\Omega \mathbf{B}^T\mathbf{D}\mathbf{B}\, d\Omega}_{\mathbf{K}_T(\mathbf{0})}\frac{1}{2}\left(\frac{\partial \boldsymbol{\varphi}_{k0}}{\partial s_j} + \frac{\partial \boldsymbol{\varphi}_{j0}}{\partial s_k}\right) + \\ &\underbrace{\frac{1}{2}\sum_{\ell=1}^{\mu}\sum_{m=1}^{\mu}\int_\Omega\left(\mathbf{B}^T\mathbf{D}\mathbf{I}_\ell\frac{\partial \mathbf{V}_0}{\partial s_k}\mathbf{S}_\ell + 2\mathbf{S}_m\frac{\partial \mathbf{V}_0}{\partial s_k}\mathbf{I}_m\mathbf{D}\mathbf{B}\right)d\Omega\,\boldsymbol{\varphi}_{j0}}_{\frac{\partial \mathbf{K}_s(\mathbf{0})}{\partial s_k}}\Bigg]s_j s_k + .. \\ = ..+\sum_{j=1}^{N}\sum_{k=1}^{N}&\left[\mathbf{K}_T(\mathbf{0})\frac{1}{2}\left(\frac{\partial \boldsymbol{\varphi}_{k0}}{\partial s_j} + \frac{\partial \boldsymbol{\varphi}_{j0}}{\partial s_k}\right) + \frac{\partial \mathbf{K}_s(\mathbf{0})}{\partial s_k}\boldsymbol{\varphi}_{j0}\right]s_j s_k + ..\end{aligned} \tag{74}$$

The internal restoring forces in (74) are expressed as a function of the tangent stiffness matrix and the secant stiffness matrix differentiated with respect to the modal co-ordinate s_k, both evaluated at zero displacements, i.e. $\mathbf{V} = \mathbf{0}$. It could be argued to replace $\mathbf{K}_T(\mathbf{0})$ with $\mathbf{K}_s(\mathbf{0})$ in the equations, as these are identical. However, from the full derivations (not shown here) with nonzero initial displacements, i.e. $s_{j0} \neq 0$, it can be seen that it is the tangent stiffness matrix that appears in the equations.

Now, by inserting the expressions in equations (73) and (74) into equation (60), the latter can be written as the vector polynomial

$$\mathbf{A} + \sum_{j=1}^{N} \mathbf{B}_j s_j + \sum_{j=1}^{N} \sum_{k=1}^{N} \mathbf{C}_{jk} s_j s_k + ... = \mathbf{0} \tag{75}$$

with the vector coefficients $\mathbf{A}$, $\mathbf{B}_j$ and $\mathbf{C}_{jk}$. If the vector polynomial in (75) should be zero for any choice of s_j, it is required that all of the vector coefficients are zero. The equations found by setting $\mathbf{A}$ equal to zero represents the EOMs; the equations found by setting $\mathbf{B}_j$ equal to zero represent the eigenvalue problem and the equations found by setting $\mathbf{C}_{jk}$ equal to zero yields the equations governing the first order modal derivatives. The latter are shown in (76) with $s_{j0} = 0$, $j \, \epsilon \, [0; N]$.

$$\left[\mathbf{K}_T(\mathbf{0}) - (\omega_{j0} + \omega_{k0})^2 \mathbf{M}\right] \frac{1}{2} \left(\frac{\partial \boldsymbol{\varphi}_{k0}}{\partial s_j} + \frac{\partial \boldsymbol{\varphi}_{j0}}{\partial s_k} \right) = \left[2 \frac{\partial \omega_{j0}}{\partial s_k} (\omega_{k0} + \omega_{j0}) \mathbf{M} - \frac{\partial \mathbf{K}_S(\mathbf{0})}{\partial s_k} \right] \boldsymbol{\varphi}_{j0} \tag{76}$$

The differentiated natural angular frequency on the right hand side of (76) is an unknown quantity. The symmetry of the governing equations is used to express this through known quantities. It is obvious that the left hand side of (76) is symmetric with respect to the subindeces j and k. In order for the equations to be consistent, this requires the right hand side to be symmetric with respect to these indeces as well. It is therefore valid that

$$\left[2 \frac{\partial \omega_{j0}}{\partial s_k} (\omega_{k0} + \omega_{j0}) \mathbf{M} - \frac{\partial \mathbf{K}_S(\mathbf{0})}{\partial s_k} \right] \boldsymbol{\varphi}_{j0} = \left[2 \frac{\partial \omega_{k0}}{\partial s_j} (\omega_{j0} + \omega_{k0}) \mathbf{M} - \frac{\partial \mathbf{K}_S(\mathbf{0})}{\partial s_j} \right] \boldsymbol{\varphi}_{k0} \tag{77}$$

Multiplying (77) through by $\boldsymbol{\varphi}_{j0}^T$ and introducing the orthogonality relationship known from linear theory, which is valid for $j \neq k$:

$$\boldsymbol{\varphi}_{j0}^T \mathbf{M} \boldsymbol{\varphi}_{k0} = 0 \tag{78}$$

the following relation is found:

$$2 \frac{\partial \omega_{j0}}{\partial s_k} (\omega_{k0} + \omega_{j0}) = \underbrace{\frac{1}{m_j} \boldsymbol{\varphi}_{j0}^T \left(\frac{\partial \mathbf{K}_S(\mathbf{0})}{\partial s_k} \boldsymbol{\varphi}_{j0} - \frac{\partial \mathbf{K}_S(\mathbf{0})}{\partial s_j} \boldsymbol{\varphi}_{k0} \right)}_{\alpha_0} \tag{79}$$

where

$$m_j = \boldsymbol{\varphi}_{j0}^T \mathbf{M} \boldsymbol{\varphi}_{j0} \tag{80}$$

By inserting the relation in (79) into (76), the complete governing system of equations in (76) consist of purely known quantities.

B. DIFFERENTIATED STIFFNESS MATRICES

Equations (42) and (50) include the secant and tangent stiffness matrices both differentiated with respect to the modal co-ordinate s_j. According to (20), $\mathbf{V}(\mathbf{s})$ is a function of $\mathbf{s}$. Thus, when differentiating the matrices with respect to s_j, only the displacements vectors are considered to be

variables. Therefore, the element local secant stiffness matrix in (16) in differentiated form becomes:

$$\frac{\partial \mathbf{k}_s(\mathbf{s})}{\partial s_j} = \int_\Omega \frac{EA}{2}\left(\mathbf{B}_\epsilon^T \frac{\partial \mathbf{v}}{\partial s_j}^T \mathbf{G} + 2\mathbf{G}\frac{\partial \mathbf{v}}{\partial s_j}\mathbf{B}_\epsilon + \mathbf{G}\left(\frac{\partial \mathbf{v}}{\partial s_j}\mathbf{v}^T + \mathbf{v}\frac{\partial \mathbf{v}}{\partial s_j}^T\right)\mathbf{G}\right) d\Omega \tag{81}$$

Furthermore, the tangent stiffness matrix in (17), when differentiated, becomes

$$\frac{\partial \mathbf{k}_T(\mathbf{s})}{\partial s_j} = \int_\Omega EA\left(\mathbf{B}_\epsilon^T \frac{\partial \mathbf{v}}{\partial s_j}^T \mathbf{G} + \mathbf{G}\frac{\partial \mathbf{v}}{\partial s_j}\mathbf{B}_\epsilon + \mathbf{G}\left(\frac{\partial \mathbf{v}}{\partial s_j}\mathbf{v}^T + \mathbf{v}\frac{\partial \mathbf{v}}{\partial s_j}^T\right)\mathbf{G} + \mathbf{B}_\epsilon \frac{\partial \mathbf{v}}{\partial s_j}\mathbf{G} + \mathbf{v}^T\mathbf{G}\frac{\partial \mathbf{v}}{\partial s_j}\mathbf{G}\right) d\Omega \tag{82}$$

where the symmetry of $\mathbf{G}$ has been utilized. In the given work (81)-(82) are evaluated at zero displacements, i.e. for $s_i = 0$, $i \in [1;N]$, and with (29) inserted. To obtain the global secant matrix and the global tangent stiffness matrix on differentiated form, all local element contributions in (81) and (82) are assembled.

REFERENCES

1. Dufour C, Andrade C, Blanger J. Real-time simulation technologies in education: a link to modern engineering methods and practices. *Proceedings of the 11th International Conference on Engineering and Technology Education*, vol. 11, Ilhus, Brazil, 2010; 114–118.
2. Barbic J, James D. Real-time subspace integration for st. venant-kirchhoff deformable models. *ACM Transactions on Graphics* 2005; **24**:982–990, doi:10.1145/1073204.1073300.
3. Saouma V, Kang DH, Haussmann G. A computational finite-element program for hybrid simulation. *Earthquake Engineering & Structural Dynamics* 2012; **41**:375–389, doi:10.1002/eqe.1134.
4. Chen C, Ricles JM, Karavasilis TL, Chae Y, Sause R. Evaluation of a real-time hybrid simulation system for performance evaluation of structures with rate dependent devices subjected to seismic loading. *Engineering Structures* 2012; **35**:71–82, doi:10.1016/j.engstruct.2011.10.006.
5. Verma M, Rajasankar J. Improved model for real-time substructuring testing system. *Engineering Structures* 2012; **41**:258–269, doi:10.1016/j.engstruct.2012.03.031.
6. Yang YS, Tsai KC, Elnashai AS, Hsieh TJ. An online optimization method for bridge dynamic hybrid simulations. *Simulation Modelling Practice and Theory* 2012; **28**:42–54, doi:10.1016/j.simpat.2012.06.002.
7. Abdelnaby AE, Frankie TM, Elnashai AS, Spencer BF, Kuchma DA, Silva P, Chang CM. Numerical and hybrid analysis of a curved bridge and methods of numerical model calibration. *Engineering Structures* 2014; **70**:234–245, doi:10.1016/j.engstruct.2014.04.009.
8. Hashemi MJ, Masroor A, Mosqueda G. Implementation of online model updating in hybrid simulation. *Earthquake Engineering and Structural Dynamics* 2014; **43**:395–412, doi:10.1002/eqe.2350.
9. Abbiati G, Bursi OS, Caperan P, Di Sarno L, Molina FJ, Paolacci F, Pegon P. Hybrid simulation of a multi-span rc viaduct with plain bars and sliding bearings. *Earthquake Engineering and Structural Dynamics* 2015; **44**:2221–2240, doi:10.1002/eqe.2580.
10. Chae Y, Kazemibidokhti K, Ricles JM. Adaptive time series compensator for delay compensation of servo-hydraulic actuator systems for real-time hybrid simulation. *Earthquake Engineering & Structural Dynamics* 2013; **42**:1697–1715, doi:10.1002/eqe.2294.
11. Chopra AK. *Dynamics of Structures: Theory and Application to Earthquake Engineering*. second edn., Prentice-Hall: New Jersey, USA, 1995.
12. Horri K, Kawahara M. A numerical analysis on the dynamic response of structures. *Proceedings of 19th Japan National Congress for Applied Mechanics* 1969; :17–22.
13. Nickell RE. Nonlinear dynamics by mode superposition. *Computer Methods in Applied Mechanics and Engineering* 1976; **7**:107–129, doi:10.1016/0045-7825(76)90008-6.
14. Niroomandi S, Alfaro I, Cueto EG, Chinesta F. Accounting for large deformations in real-time simulations of soft tissues based on reduced-order models. *Computer Methods and Programs In Boimedicine* 2012; **105**:1–12, doi: 10.1016/j.cmpb.2010.06.012.
15. Darby AP, Blakeborough A, Williams MS. Improved control algorithm for real-time substructure testing. *Earthquake Engineering & Structural Dynamics* 2001; **30**:431–448, doi:10.1002/eqe.18.
16. Blakeborough A, Williams MS, Darby AP, Williams DM. The development of real-time substructure testing. *Philosophical Transactions of the Royal Society A: Mathematical, Physical and Engineering Sciences* 2001; **359**:1869–1891, doi:10.1098/rsta.2001.0877.
17. Lülf FA, Tran DM, Ohayon R. Reduced bases for nonlinear structural dynamic systems: A comparative study. *Journal of Sound and Vibration* 2013; **332**:3897–3921, doi:10.1016/j.jsv.2013.02.014.
18. Idelsohn SR, Cardona A. Recent advances in reduction methods in nonlinear structural dynamics. *Proceedings of the Second International Conference on: Recent Advances in Structural Dynamics*, vol. 2, University of Southampton, England, 1984; 475–482.
19. Wilson EL, Yuan MW, Dickens JM. Dynamic analysis by direct superposition of ritz vectors. *Earthquake Engineering & Structural Dynamics* 1982; **10**:813–821, doi:10.1002/eqe.4290100606.

20. Chaturantabut S, Sorensen DC. Nonlinear model reduction via discrete empirical interpolation. *SIAM Journal on Scientific Computing* 2010; **32**:2737–2764, doi:10.1137/090766498.
21. Carlberg K, Bou-Mosleh C, Farhat C. Efficient non-linear model reduction via a least-squares petrov-galerkin projection and compressive tensor approximations. *International Journal for Numerical Methods in Engineering* 2011; **86**:155–181, doi:10.1002/nme.3050.
22. Amsallem D, Zahr MJ, Farhat C. Nonlinear model order reduction based on local reduced-order bases. *International Journal for Numerical Methods in Engineering* 2012; **92**:891–916, doi:10.1002/nme.4371.
23. Idelsohn SR, Cardona A. A reduction method for nonlinear structural dynamic analysis. *Computer Methods in Applied Mechanics and Engineering* 1985; **49**:253–279, doi:10.1016/0045-7825(85)90125-2.
24. Idelsohn SR, Cardona A. A load-dependent basis for reduced nonlinear structural dynamics. *Computers & Structures* 1985; **20**:203–210, doi:10.1016/0045-7949(85)90069-0.
25. Weeger O, Wever U, Simeon B. Nonlinear frequency response analysis of structural vibrations. *Computational Mechanics* 2014; **54**:1477–1495, doi:10.1007/s00466-014-1070-9.
26. Weeger O, Wever U, Simeon B. On the use of modal derivatives for nonlinear model order reduction. *International Journals for Numerical Methods in Engineering* 2016; **108**:1579–1602, doi:10.1002/nme.5267.
27. Slaats PMA, de Jongh J, Sauren AAHJ. Model reduction tools for nonlinear structural dynamics. *Computer & Structures* 1995; **54**:1155–1171, doi:10.1016/0045-7949(94)00389-K.
28. Tiso P, Jansen E, Abdalla M. Reduction method for finite element nonlinear dynamic analysis of shells. *Aiaa Journal* 2011; **49**:2295–2304, doi:10.2514/1.J051003.
29. Poulsen PN, Damkilde L. A flat triangular shell element with loof nodes. *International Journal for Numerical Methods in Engineering* 1996; **39**:3867–3887, doi:10.1002/(SICI)1097-0207(19961130)39:22⟨3867::AID-NME28⟩3.0.CO;2-H.
30. Inman DJ. *Engineering Vibrations*. third edn., Pearson Education: New Jersey, USA, 2009.
31. Cook RD, Malkus DS, Plesha ME, Witt RJ. *Concepts and Applications Of Finite Element Analysis*. fourth edn., John Wiley & Sons: New York, USA, 1974.
32. Belytschko T, Liu WK, Moran B. *Nonlinear Finite Elements for Continua and Structures*. first edn., John Wiley & Sons: Chicester, England, 2000.
33. Krenk S. *Non-linear Modeling and Analysis of Solids and Structures*, vol. 1. first edn., Cambridge University Press: Cambridge, UK, 2009.